

Electronic Supporting Information

Building responsive materials by assembling {Fe₄Co₄} switchable molecular cubes

by Q. X. Pham *et al.*

1. Technical Details	2
2. Synthesis of ditopic ligand.....	4
3. ¹ H and ¹³³ Cs NMR spectra of the pro-cube and model cube and polymer	6
4. Mass spectrometry	10
5. Magnetic Measurements	11
6. Photomagnetic Measurements of the model cubes	12
7. Pictures of the reaction media during the syntheses and SEM image of the polymeric material....	14
8. Crystallographic details of the paramagnetic cubic model	16
9. Powder-XRD diffractogram of the precipitated polymeric compound.	19
10. Thermo-Gravimetric Analyses.....	20

^a Sorbonne Université, CNRS, Institut Parisien de Chimie Moléculaire, F-75005 Paris, France

^b Sorbonne Université, CNRS, Physico-chimie des électrolytes et nano-systèmes interfaciaux, PHENIX, F-75005 Paris, France

^c Réseau sur le Stockage Electrochimique de l'Energie (RS2E), FR CNRS 3459, 80039 Amiens, France

^d X-ray Science Division, Advanced Photon Source, Argonne National Laboratory, 9700 South Cass Avenue, Argonne, Illinois 60439, United States

^e Université Paris-Saclay, CNRS, Institut Chimie Moléculaire et Matériaux d'Orsay, Orsay, France

^f Institut des Matériaux Poreux de Paris, Ecole Normale Supérieure, ESPCI Paris, CNRS, PSL University, 75005, Paris, France

1. Technical Details

FT-IR spectra were collected in the 200-4000 cm^{-1} range. Measurements were carried out on a Vertex 70 Bruker instrument using the attenuated total reflection (ATR) technique on solid samples (with a 4 cm^{-1} resolution). The intensity of the absorption band is indicated as vw (very weak), w (weak), m (medium), s (strong), vs (very strong), and br (broad).

NMR Spectroscopy Measurements. All the solution and solid-state NMR spectra were measured with Bruker Avance III spectrometers at 300 K. The solid-state NMR spectra were acquired using the magic angle spinning (MAS) technique, by rotating the sample at $\theta \approx 54.74^\circ$ respective to the magnetic field. The acquired spectra showed isotropic chemical shift and a spinning sideband pattern, regularly spaced by the spinning rate, n_r . The ^{133}Cs chemical shift were measured by using CsNO_3 as reference.

Solid-state UV vis of the network was performed using linear transmission measurement using JASCO V670 spectrometer at room temperature. The network powder was mixed with KBr to have a thin, homogeneous pellet (thickness is less than 3 mm to ensure no significant change in beam size). The baseline correction was performed on air with no sample mounted. After that, the sample was mounted and the UV scan was performed.

Solution UV-vis absorption spectra were measured in the range between 200-2000 nm in a CARY 4000 UV-vis spectrophotometer.

Elemental analyses (C, H, N, S) were carried out by combustion analysis using a vario MICRO cube apparatus from Elementar.

Mass spectrometric analyses. The ESI-MS experiments were undertaken on a micro-TOF Bruker mass spectrometer, in positive ionization mode with a spray voltage of 4.5kV. The ion transfer capillary was held at 180°C. The measurements were operated in acetonitrile by direct infusion from a Harvard syringe pump to the ESI-source at a rate of 100 $\mu\text{L}\cdot\text{min}^{-1}$.

X-Ray crystal structure determination. Several single crystals were mounted and tested in the lab and diffraction peaks were weak. The data collection for cube model was then carried out at the CRISTAL beamline (synchrotron SOLEIL, Paris) using the synchrotron radiation source ($\lambda = 0.67138 \text{ \AA}$). The experiment temperature ($T = 100 \text{ K}$) was reached with a gas streamer (CryoIndustries of America), crystal-to-detector distance of 80 mm. Wavelength was selected with a double crystal monochromator (Si 111 crystals) and sagittal (horizontal), focalization was achieved by bending the second crystal of the monochromator. The beam attenuation was performed using Cu foils of different thicknesses inserted in the incident beam. Data collection strategies were generated with the CrysAlisPro CCD package and adapted to the peculiar angular constraints of the CRISTAL 4C

Newport diffractometer. Unit-cell parameters refinement and data reduction were carried out with CrysAlisPro RED.² The structure was solved using SHELXT-14³ implemented in Olex2 program.⁴ The refinements were then carried out with SHELXL⁵, by full-matrix least squares minimization and difference Fourier methods.

CCDC 2072191 contain the supplementary crystallographic data for this paper. The data can be obtained free of charge from The Cambridge Crystallographic Data Centre via www.ccdc.cam.ac.uk/structures.

The powder X-ray Diffraction (PXRD) data were recorded on a high-throughput Bruker D8 Advance diffractometer working on transmission mode and equipped with a focusing Göbel mirror producing CuK α radiation ($\lambda = 1.5418 \text{ \AA}$) and a LynxEye detector.

Nitrogen porosimetry data were collected on a Micromeritics Tristar instrument at 77 K (pre-activating samples at 150 °C under vacuum, 6 hours).

Thermogravimetric Analysis (TGA) was carried out with a TGA analyser (TAI instrument, SDT Q600) at a rate of 2 °C min⁻¹ under a dinitrogen flow (100mL/min).

SEM images were recorded with FEI Magellan 400 scanning electron microscope equipped with and Oxford **EDS** (energy dispersive spectroscopy) probe.

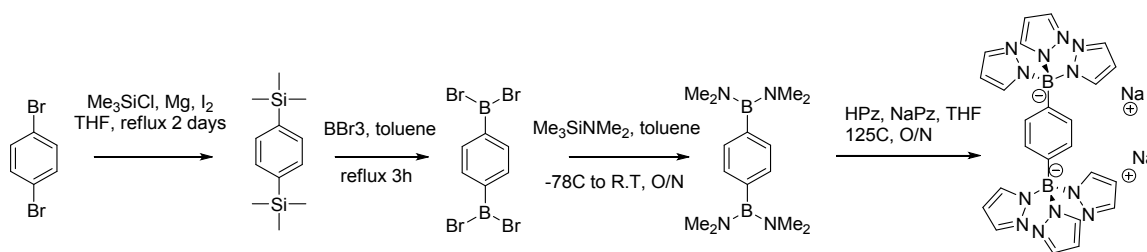
² CrysAlisPro 1.171.40.64 (Rigaku Oxford Diffraction, 2015)

³ Sheldrick, G. M. SHELXT – Integrated space-group and crystal-structure determination. *Acta Cryst.*, A71, 3-8 (2015)

⁴ Dolomanov O. V., L. J. Bourhis, R. J. Gildea, J. A. Howard, H.; Puschmann, *OLEX2: a complete structure solution, refinement and analysis program. J. Appl. Crystallogr.*, 42, 339-341 (2009)

⁵ Sheldrick, G. M., Crystal Structure Refinement with SHELXL. *Acta Cryst.*, C71, 3–8. (2015).

2. Synthesis of ditopic ligand



Scheme of the synthesis of the ditopic tris(pyrazolyl) ligand

All chemicals were purchased from standard chemicals' providers and used as received. Reactions were carried out in inert atmosphere.

The 1,4-bis-(trispyrazolylborate) benzene (Tp-Ar-Tp) has been synthesized in four steps as described as previously.⁶ However, in that previous work the ligand was not isolated and characterized but directly used to obtain a Thallium(I) complex. This is certainly related to the relative instability of the uncoordinated ligand toward hydrolysis. In previous works, we observed that in these ligands (third generation of scorpionate functionalized with aryl group on the boron), the coordination of the pyrazolyl groups to a metal ion prevent the hydrolysis.⁷ In this work, we isolated the ligand with ca. 10% of NaPz starting material. Any attempt of purification before lead to some partial degradation due to of the ligand we thus used as it is too.

Synthesis of compound 1,4-bis(trimethylsilyl)benzene

1,4-dibromobenzene (12 g, 50.5 mmol, 1 eq) was dissolved in dried THF (50 mL). A stirred suspension of Me₃SiCl (12.8 mL, 110.4 mmol, 2.4 eq), Mg (2.48 g, 100 mmol, 2 eq) and I₂ in dried THF (100 mL) was added dropwise at 0 °C. After stirring one night at r.t., the reaction mixture was heated under reflux for 48h. 15 mL of a saturated aqueous solution of NH₄Cl and 60 mL of water were added. The organic phase was separated and washed with water (2 x 30 mL), and the aqueous phase was extracted with THF (3 x 30 mL). The combined organic phases were dried over Na₂SO₄, filtered and evaporated. Product was further purified by recrystallization in EtOH to give 6.5 g of product (59%). ¹H NMR (400 MHz, CDCl₃): δ= 7.52 (s, 4H, Ar-H), 0.27 ppm(s, 18H, CH₃) which is matched with reported compound.⁶

⁶ Moerlein, S., Synthesis and spectroscopic characteristics of aryltrimethyl-silicon,-germanium, and-tin compounds. *Journal of organometallic chemistry* **1987**, 319 (1), 29-39.

⁷ A Benchohra, Magnetic molecular switches: From their synthesis to their integration into hybrid (nano)materials, Ph.D., Sorbonne University, Feb. **2019**; A Benchohra et al. *Angew. Chemie. Int. Ed.* **2021**, 16, 8803-8807.

Synthesis of compound sodium 1,4-bis-(trispirazolyborate) benzene (ditopic)

BBr_3 (1.5 mL, 15.965 mmol, 2.9 eq) was added dropwise to a stirred solution of 1,4-bis(trimethylsilyl)benzene (1.2 g, 5.4 mmol, 1 eq) in toluene (8 mL) in a Schlenk flask. The resulting solution was heated to reflux for 3h. The removal of all the volatile materials under vacuum at 50 °C gave a yellow solid. The resulting solid was dissolved in toluene (10 mL) and $\text{Me}_3\text{SiNMe}_2$ (3.5 mL, 21.58 mmol, 4 eq) was added dropwise at -78 °C. After 2h at -78 °C, the reaction mixture was allowed to warm to r.t. and stirred overnight. All the volatiles were removed under reduced pressure and the yellow residue was dried under vacuum. The resulting solid was dissolved in toluene (20 mL) and a mixture of neat pyrazolide (1.47 g, 21.58 mmol, 4 eq) and neat sodium pyrazolate (0.975 g, 10.79 mmol, 2 eq) in THF (15 mL) was added at room temperature. After the suspension had been heated to reflux for 16h, the suspension was concentrated under reduced pressure. The beige precipitate was filtrated hot on a frit and washed with hot toluene (2 x 20 mL) and hexane (3 x 20 mL). The off-white resulting solid was dried under vacuum at 50 °C during 1h to remove excess pyrazole. The resulting white solid appears in $^1\text{H-NMR}$ as the desired 1,4-bis-(trispirazolyborate)benzene and NaPz as an impurity. Yield after 3 steps: 1.7 g (51%). This mixture has been used without further purification. $^1\text{H NMR}$ (400 MHz, DMSO-d_6): δ = 7.37 (d, 6H, pz), 7.06 (d, 6H, pz), 6.81 (s, 4H, Ar-H), 5.97 ppm (t, 6H, pz) which is matched with reported compound.⁸² δ 7.60 and 6.26 ppm peaks belong to remaining NaPz.

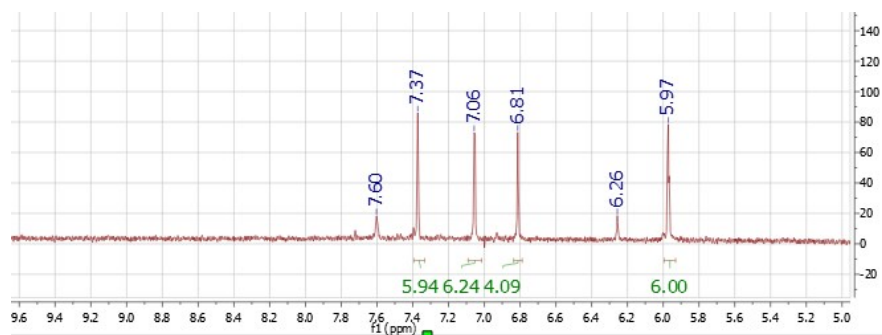


Figure S1. $^1\text{H NMR}$ of ditopic ligand in 5-10 ppm range in DMSO-d_6 .

⁸ Bieller, S.; Zhang, F.; Bolte, M.; Bats, J. W.; Lerner, H.-W.; Wagner, M., Bitopic bis- and tris (1-pyrazolyl) borate ligands: syntheses and structural characterization. *Organometallics* **2004**, 23 (9), 2107-2113.

3. ^1H and ^{133}Cs NMR spectra of the pro-cube and model cube and polymer

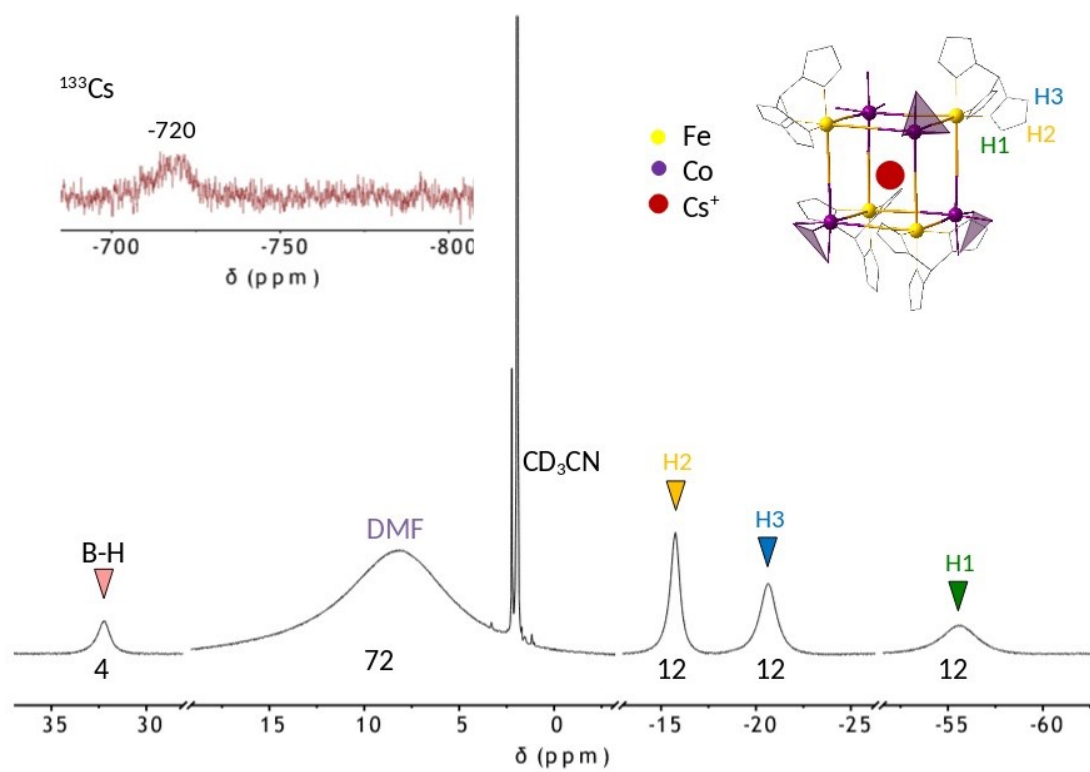


Figure S2. ^1H and ^{133}Cs NMR (inset on the left) of pro-cube (with Cs) in CD_3CN at 300K (9.4 T).

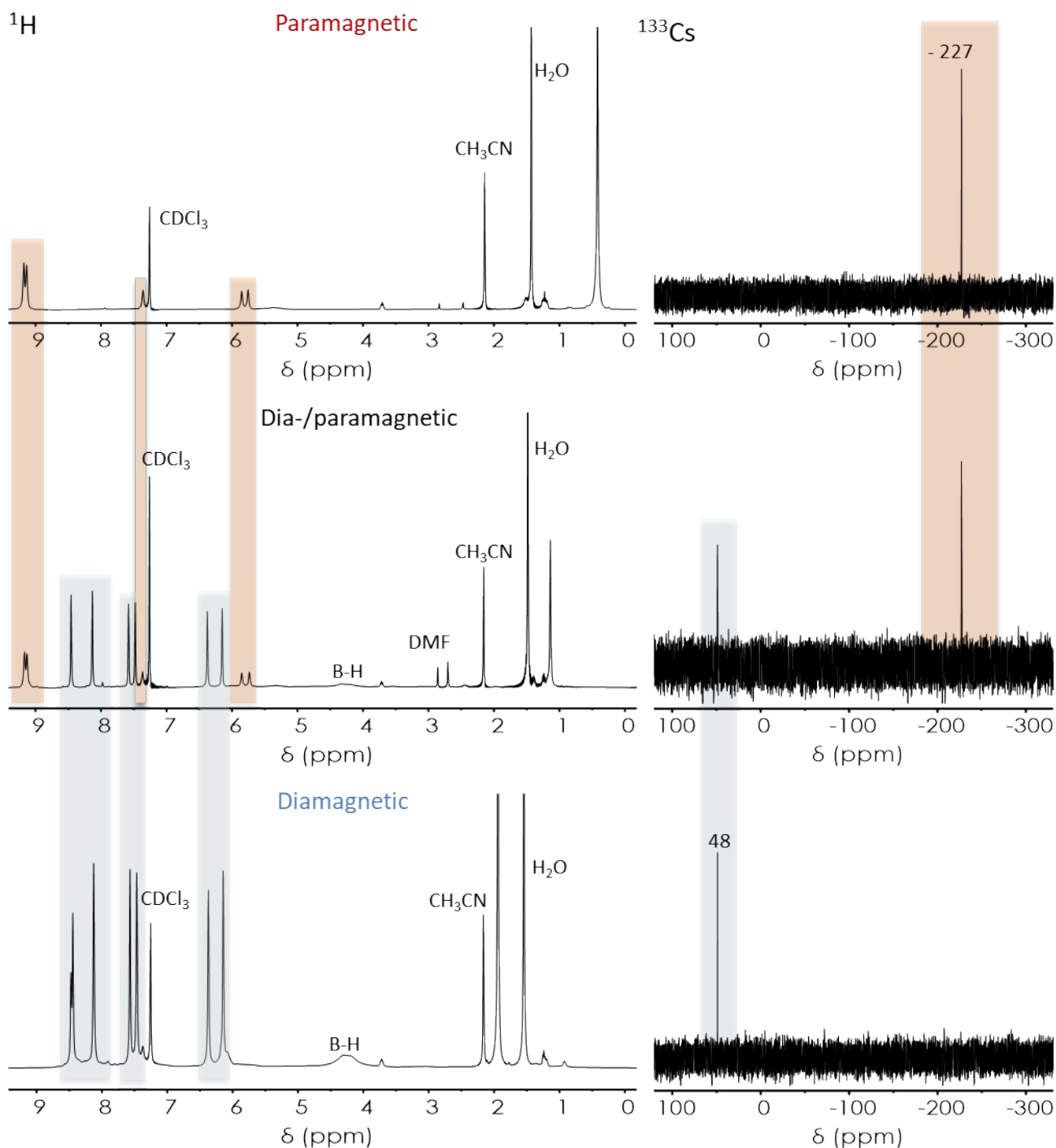


Figure S3. ^1H (left) and ^{133}Cs (right) NMR spectra of the $\text{Cs}_2\text{C}[\{\text{Fe}^{\text{II}}(\text{Tp})(\text{CN})_3\}_4\{\text{Co}^{\text{III}}(\text{Tp})_4\}]$ cubic model recorded in CD_3Cl at 300K (9.4 T): directly after the synthesis (top) only the paramagnetic $\{\text{Fe}^{\text{II}}_4\text{Co}^{\text{III}}_3\text{Co}^{\text{II}}\}$ state is observed as only the 18 expected signals are detected. After two days (middle), beside the peaks of the $\{\text{Fe}^{\text{II}}_4\text{Co}^{\text{III}}_3\text{Co}^{\text{II}}\}$ paramagnetic cube, additional diamagnetic peaks attributed to the $\{\text{Fe}^{\text{II}}_4\text{Co}^{\text{III}}_4\}$ diamagnetic cube appear. After leaving the sample in air for one week (bottom), the paramagnetic complex has been oxidized and fully converted into the diamagnetic $\{\text{Fe}^{\text{II}}_4\text{Co}^{\text{III}}_4\}$ state.

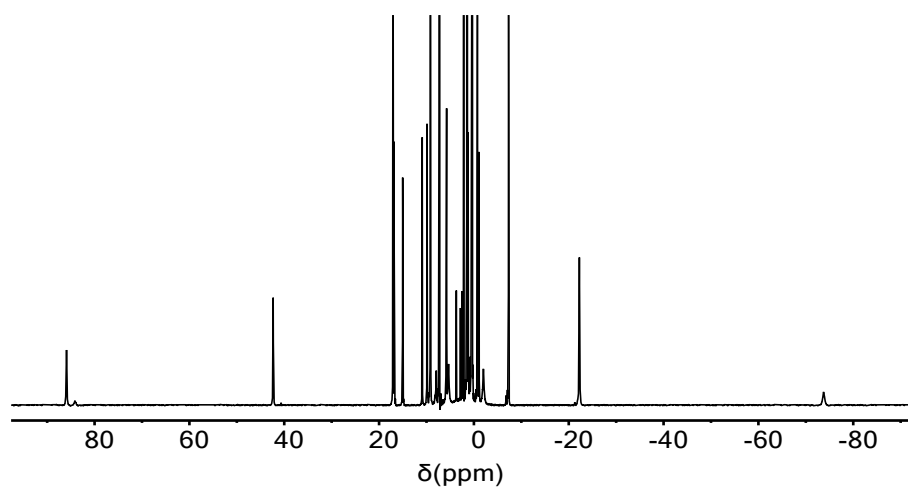


Figure S4. Full ^1H NMR spectrum of the paramagnetic $\text{Cs}_2\{[\text{Fe}(\text{Tp})(\text{CN})_3]_4[\text{Co}^{\text{II}}(\text{Tp})][\text{Co}^{\text{III}}(\text{Tp})]_3\}$ cubic model recorded in CD_3Cl at 300 K (9.4 T).

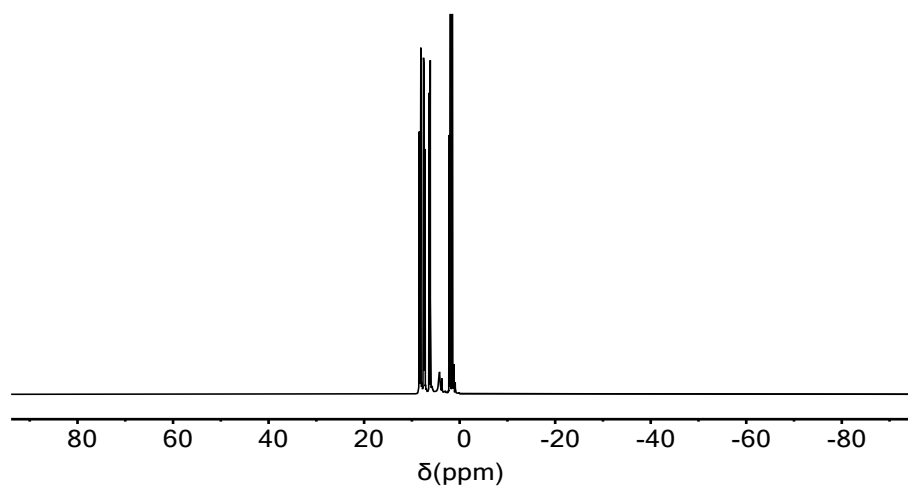


Figure S5. ^1H NMR spectrum of the diamagnetic $\text{Cs}_2\{[\text{Fe}(\text{Tp})(\text{CN})_3]_4[\text{Co}^{\text{III}}(\text{Tp})]_4\}$ cube recorded in CD_3Cl at 300 K (9.4 T).

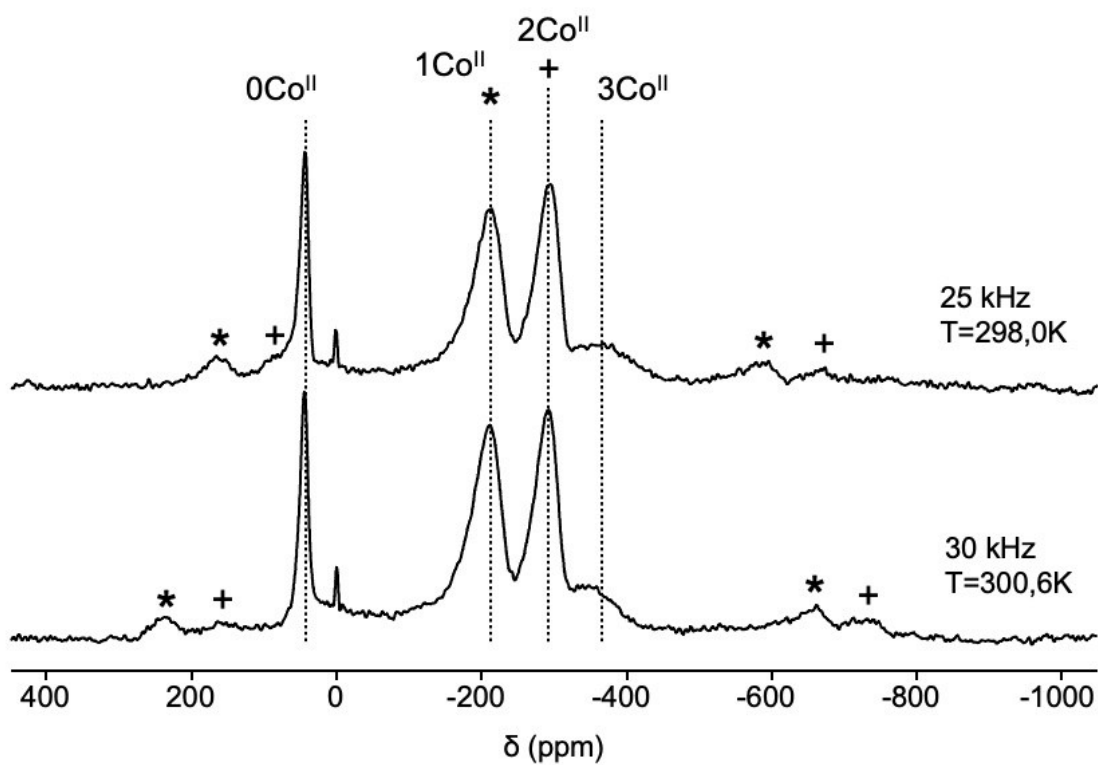


Figure S6. Solid-state ^{133}Cs NMR spectra of the polymeric material $\text{Cs}\llbracket\{\text{Fe}(\text{Tp})(\text{CN})_3\}_4\{\text{Co}^{\text{II}}(\text{Tp})\}_4\rrbracket$ acquired in echo MAS. The dotted lines indicate distinct ^{133}Cs isotropic signals ascribed to distinct $\text{Cs}\llbracket\{\text{Fe}^{\text{II}}_4\text{Co}^{\text{II}}_x\text{Co}^{\text{I}}_{(4-x)}\}\rrbracket$ cubic units. The small signals at periphery, which position depend on the MAS' speed are the side bands of the

4. Mass spectrometry

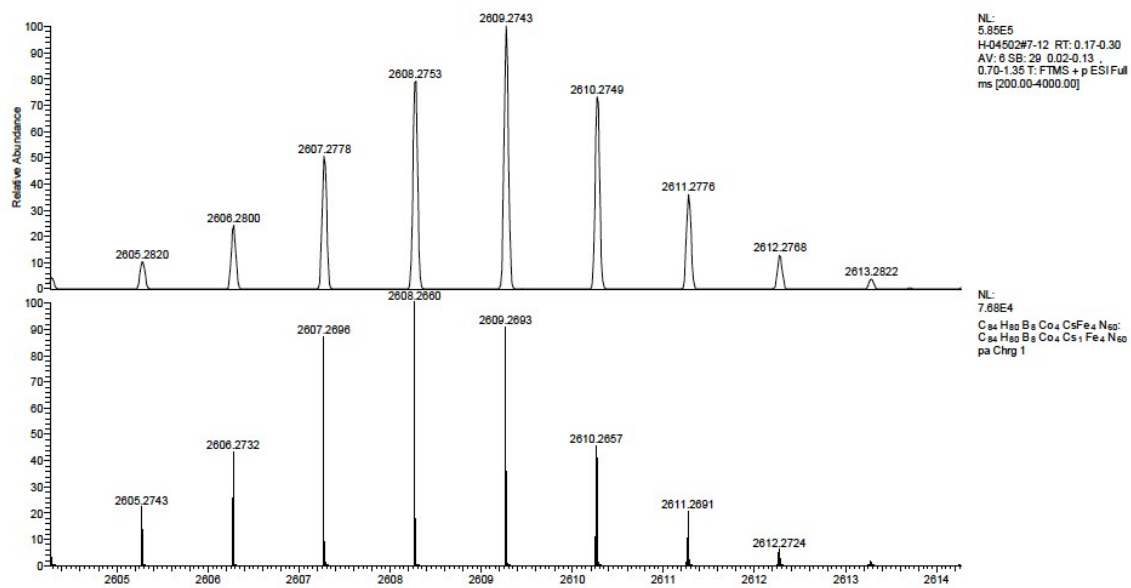
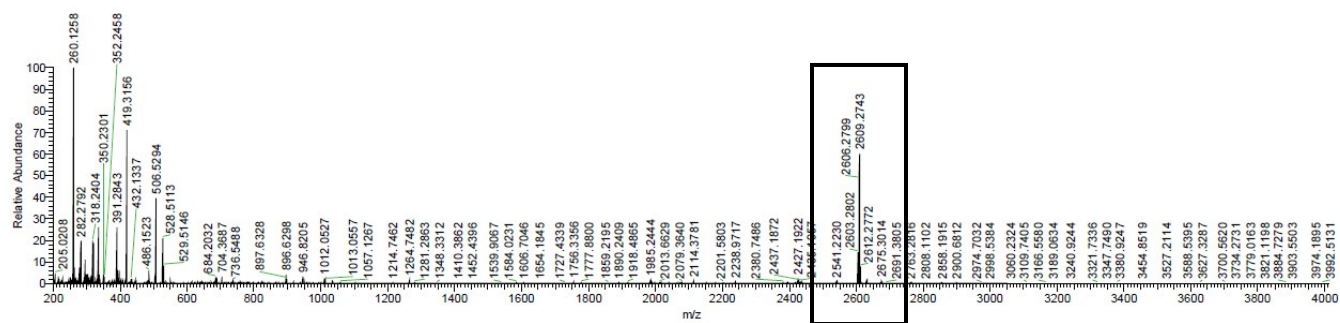


Figure S7. Full ESI Mass spectrum of the $\text{CsC}\{[\text{Fe}(\text{Tp})(\text{CN})_3]_4[\text{Co}(\text{Tp})]_4\}$ cube (top) and zoom on the isotopic massif.

5. Magnetic Measurements

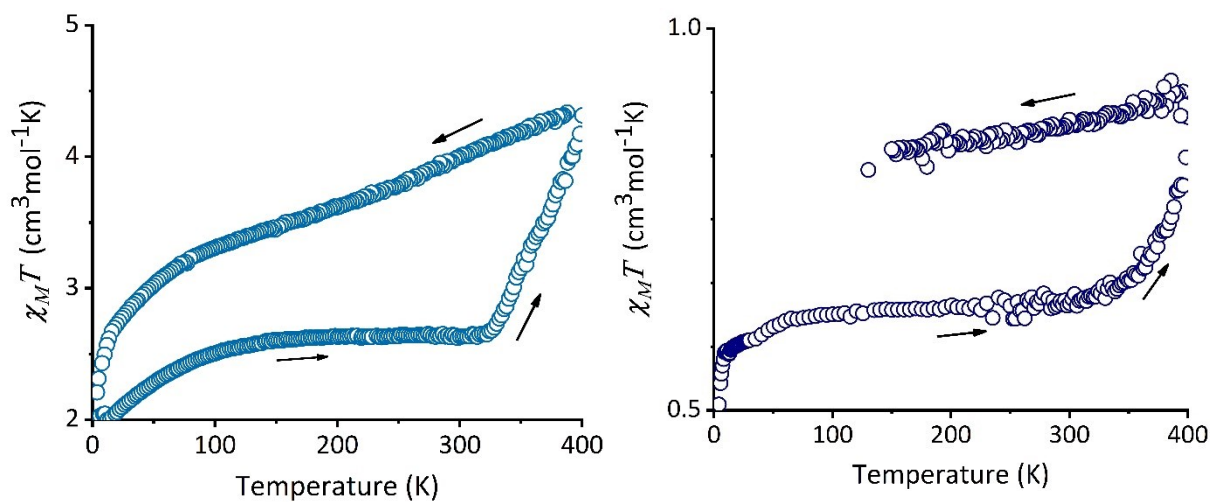


Figure S8. $\chi_M T$ versus T curve measured at 2 K/min of freshly filtered crystals of the paramagnetic (left) and diamagnetic (right) $\text{Cs}\{[\text{Fe}(\text{Tp})(\text{CN})_3]_4[\text{C}(\text{Tp})_4]\}$ showing a partial, irreversible ETCST above 300 K at $H = 1$ T.

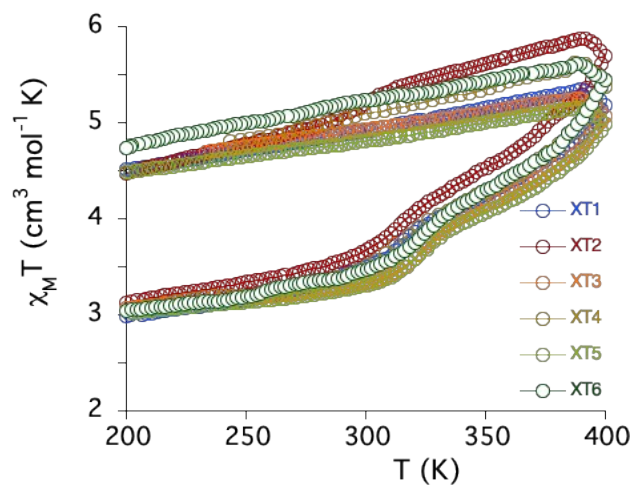


Figure S9. $\chi_M T$ versus T curves measured on water-washed samples of the network.

6. Photomagnetic Measurements of the model cubes

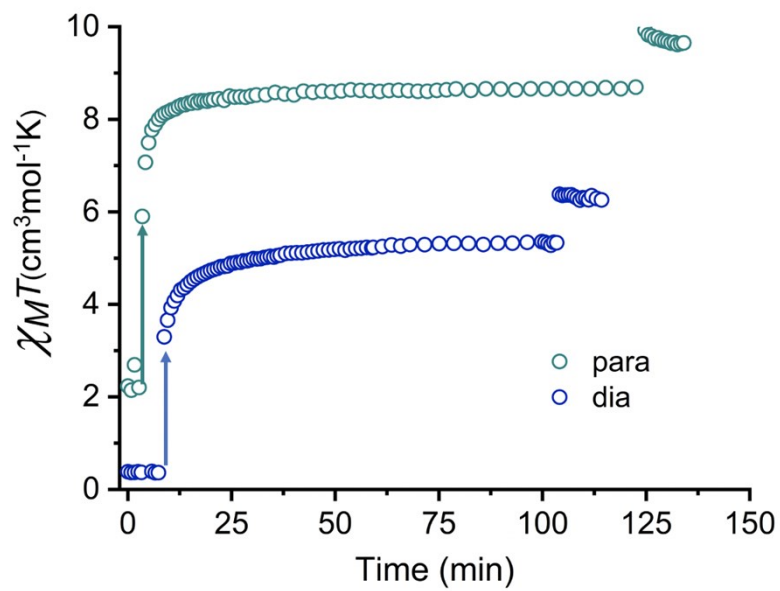


Figure S10. $\chi_M T$ versus times of the diamagnetic (blue) and paramagnetic (red) model cubes. The arrows are located at the beginning of the light irradiation.

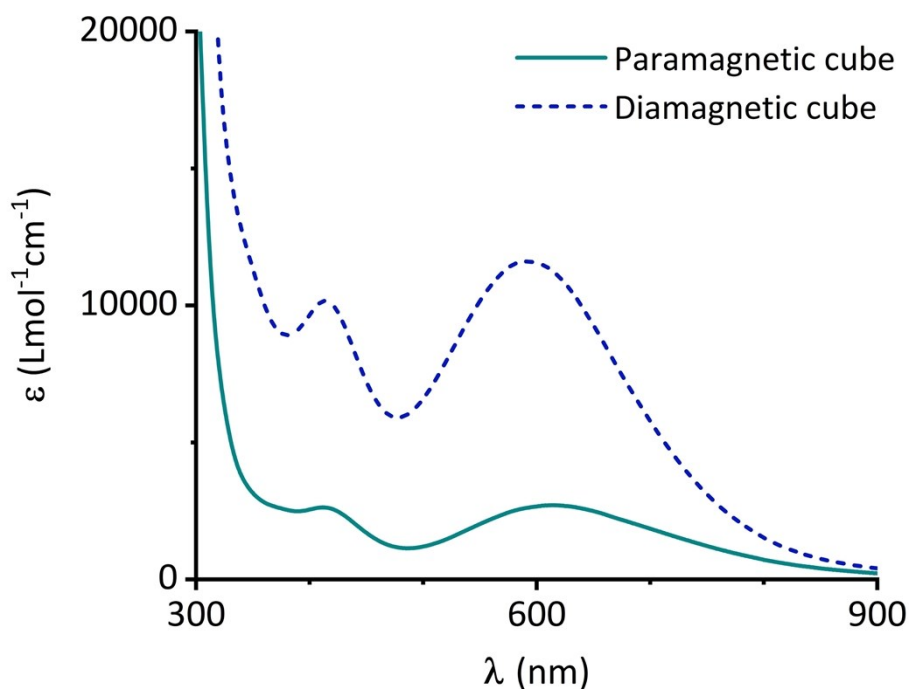


Figure S11. UV-vis spectra of the paramagnetic and diamagnetic- $\text{Cs}_2\{[\text{Fe}(\text{Tp})(\text{CN})_3]_4[\text{Co}(\text{Tp})]_4\}$ molecular model in 0.1 mM CH_2Cl_2 solution.

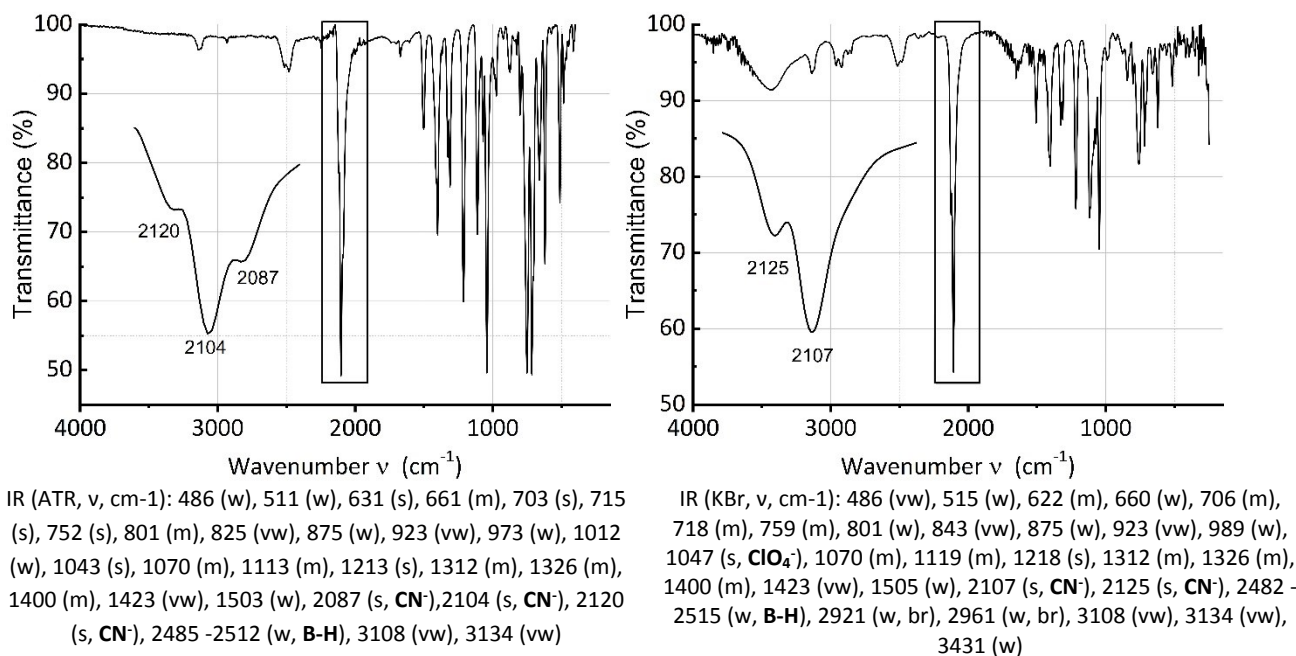


Figure S12. FT-IR-spectra of the paramagnetic (left) and diamagnetic (right) $\text{Cs}_2\{[\text{Fe}(\text{Tp})(\text{CN})_3]_4[\text{Co}^{\text{III}}(\text{Tp})]_4\}$ molecular model.

7. Pictures of the reaction media during the syntheses and SEM image of the polymeric material

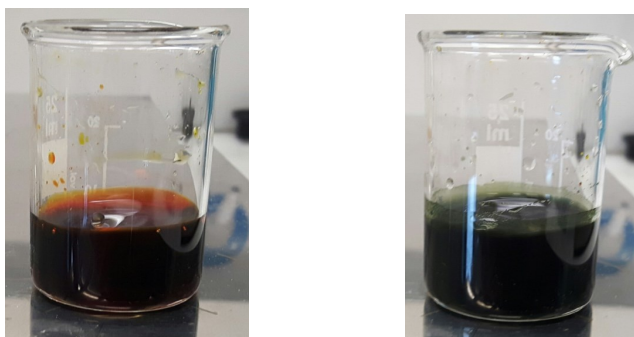


Figure S13a. pro-cube solution after adding Cs(left); precipitates after adding Tp^- ligand in DMF (right).

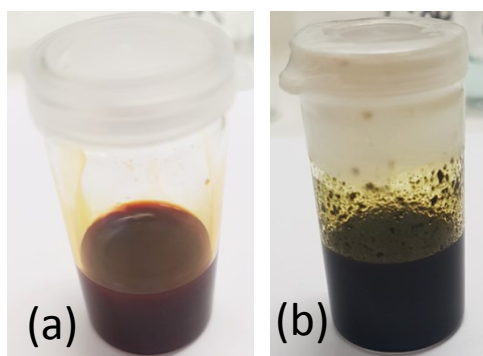


Figure S13b. Pro-cube in DMF solution after adding Cs (a); precipitates after adding ditopic ligand and sonication (b).



Figure S13c. NMR test tubes of the paramagnetic (left) and diamagnetic cubic models (right) in CD_2Cl_2 .

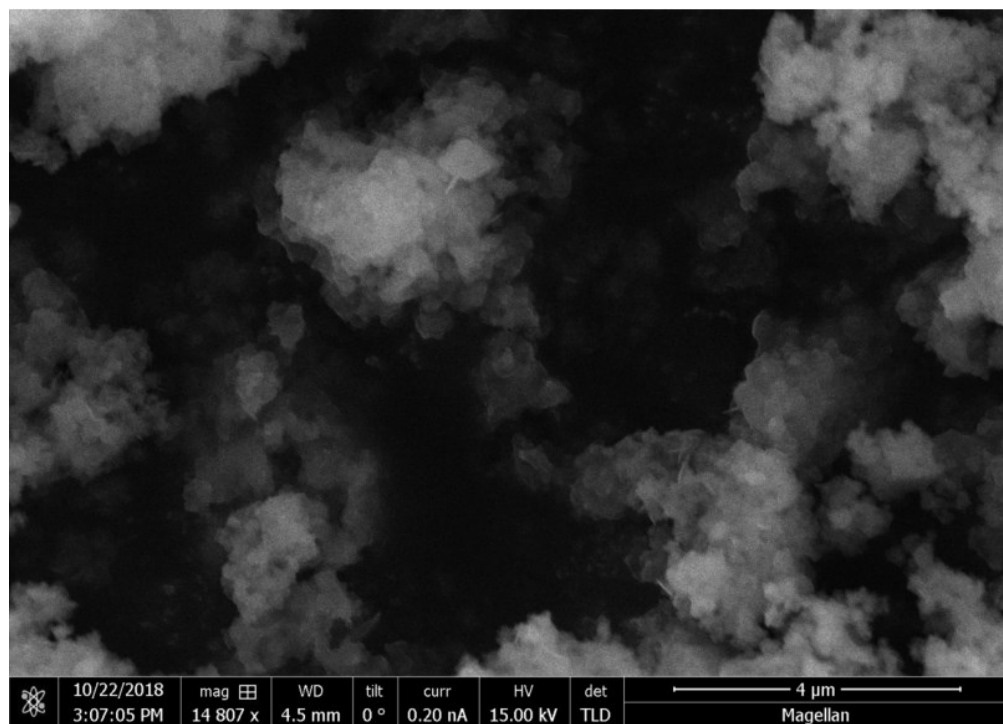
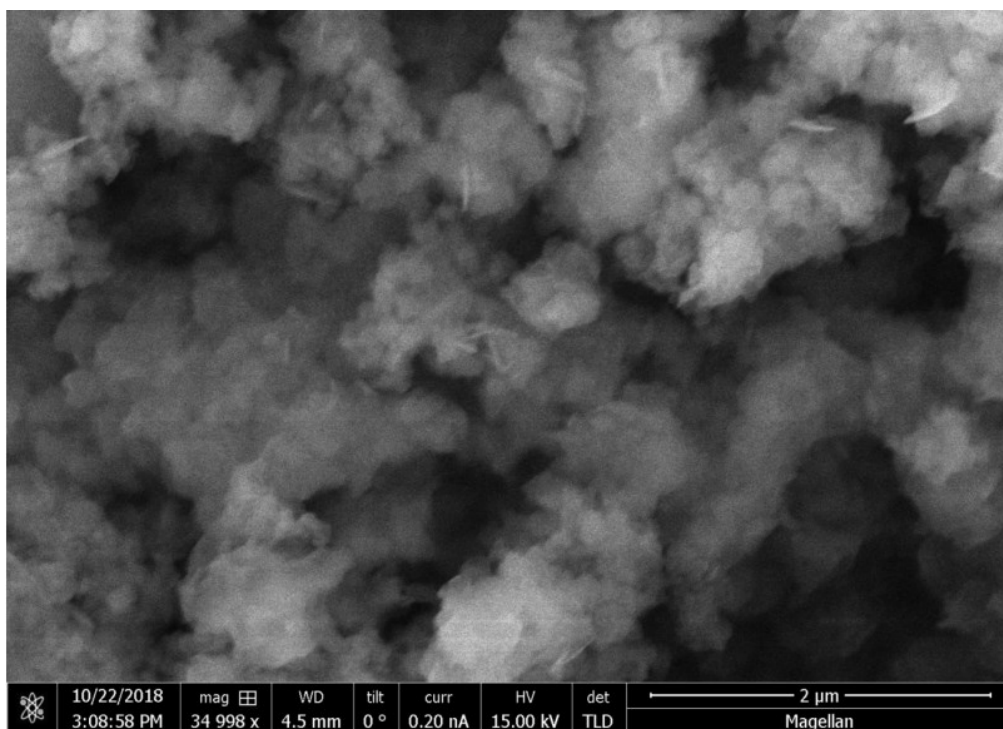


Figure S14. SEM images of the polymeric network.

8. Crystallographic details of the paramagnetic cubic model

Table S1. Crystal data and structure refinement for the model cube

Identification code	jpg407
	$C_{84}H_{80}B_8CO_4CsFe_4N_{60}$, 14(C_2H_3N), H_2O
Empirical formula	$C_{112}H_{124}B_8CO_4CsFe_4N_{74}O$
Formula weight	3201.35
Temperature/K	100
Crystal system	orthorhombic
Space group	Pbca
a/Å	24.0255(2)
b/Å	22.6715(2)
c/Å	27.0718(3)
$\alpha/^\circ$	90
$\beta/^\circ$	90
$\gamma/^\circ$	90
Volume/Å ³	14745.8(3)
Z	4
ρ_{calc}/cm^3	1.442
μ/mm^{-1}	1.066
F(000)	6516.0
Crystal size/mm ³	0.11 × 0.09 × 0.09
Radiation	synchrotron ($\lambda = 0.67138$)
2 θ range for data collection/ $^\circ$	3.262 to 51.69
Index ranges	$-30 \leq h \leq 31$, $-28 \leq k \leq 29$, $-35 \leq l \leq 35$
Reflections collected	246364
Independent reflections	16882 [$R_{int} = 0.0952$, $R_{sigma} = 0.0317$]
Data/restraints/parameters	16882/26/969
Goodness-of-fit on F^2	1.117
Final R indexes [$I \geq 2\sigma(I)$]	$R_1 = 0.0595$, $wR_2 = 0.1409$
Final R indexes [all data]	$R_1 = 0.0756$, $wR_2 = 0.1521$
Largest diff. peak/hole / e Å ⁻³	1.65/-0.72

Note: In this crystal structure, the Fe and Co metal ions are not distinguishable as the cubic molecules shows a mirror plane between two opposite faces. Only averaged bond distances are discussed in the main text.

Table S2. Table of metal-ligand distances (in Å) around metals of the cube (M= Fe/Co)

M1	N1	1.926(4)
M1	N2	1.917(4)
M1	N3	1.919(4)
M1	N1A	1.982(4)
M1	N3A	1.990(4)
M1	N5A	1.993(4)
M2	N4	1.942(4)
M2	N5	1.944(4)
M2	N6 ¹	1.930(4)
M2	N1B	2.005(4)
M2	N3B	2.006(4)
M2	N5B	2.002(4)
M3	N7	1.953(4)
M3	N8	1.935(4)
M3	N9 ¹	1.947(4)
M3	N1C	2.008(4)
M3	N3C	1.999(4)
M3	N5C	2.011(4)
M4	N10	1.904(4)
M4	N11	1.901(4)
M4	N12	1.910(4)
M4	N1D	1.966(4)
M4	N3D	1.976(3)
M4	N5D	1.975(4)

Table S3. Table of angles (in degrees) around metals of the cube

N1	M1	N1A	89.83(15)	N7	M3	N1C	179.03(15)
N1	M1	N3A	91.96(15)	N7	M3	N3C	91.54(15)
N1	M1	N5A	177.56(15)	N7	M3	N5C	92.20(16)
N2	M1	N1	90.12(15)	N8	M3	N7	90.51(15)
N2	M1	N3	89.65(15)	N8	M3	N1C	90.44(15)
N2	M1	N1A	90.78(15)	N8	M3	N3C	177.01(14)
N2	M1	N3A	177.11(15)	N8	M3	N5C	91.36(15)
N2	M1	N5A	91.31(15)	N9 ¹	M3	N7	90.82(15)
N3	M1	N1	90.51(15)	N9 ¹	M3	N1C	89.36(15)
N3	M1	N1A	179.45(16)	N9 ¹	M3	N3C	91.43(14)
N3	M1	N3A	92.34(15)	N9 ¹	M3	N5C	176.32(15)
N3	M1	N5A	91.47(15)	N1C	M3	N5C	87.58(16)
N1A	M1	N3A	87.22(16)	N3C	M3	N1C	87.50(15)
N1A	M1	N5A	88.17(15)	N3C	M3	N5C	86.39(14)
N3A	M1	N5A	86.54(15)	N7	M3	N1C	179.03(15)
N4	M2	N5	90.47(15)	N10	M4	N12	90.21(14)
N4	M2	N1B	177.33(15)	N10	M4	N1D	178.72(15)
N4	M2	N3B	90.20(15)	N10	M4	N3D	91.70(14)
N4	M2	N5B	91.89(15)	N10	M4	N5D	90.74(15)
N5	M2	N1B	91.97(15)	N11	M4	N10	90.11(15)
N5	M2	N3B	178.24(15)	N11	M4	N12	90.49(15)
N5	M2	N5B	90.91(15)	N11	M4	N1D	90.60(14)
N6 ¹	M2	N4	89.85(15)	N11	M4	N3D	177.59(15)
N6 ¹	M2	N5	90.63(15)	N11	M4	N5D	90.76(15)
N6 ¹	M2	N1B	91.20(14)	N12	M4	N1D	90.85(14)
N6 ¹	M2	N3B	91.00(15)	N12	M4	N3D	91.09(15)
N6 ¹	M2	N5B	177.67(14)	N12	M4	N5D	178.43(15)
N1B	M2	N3B	87.33(15)	N1D	M4	N3D	87.56(14)
N5B	M2	N1B	86.99(15)	N1D	M4	N5D	88.19(14)
N5B	M2	N3B	87.44(15)	N5D	M4	N3D	87.63(14)

Table S4. Distances between Cs atom and metallic atoms Fe/M (in Å)

M1	M2	5.0125(8)
M2	M3	5.0257(8)
M4	M3	4.9967(8)
M4	M1	4.9654(7)
Cs1	M4	4.3080(5)
Cs1	M1	4.3298(6)
Cs1	M2	4.3535(6)
Cs1	M3	4.3370(5)

9. Powder-XRD diffractogram of the precipitated polymeric compound.

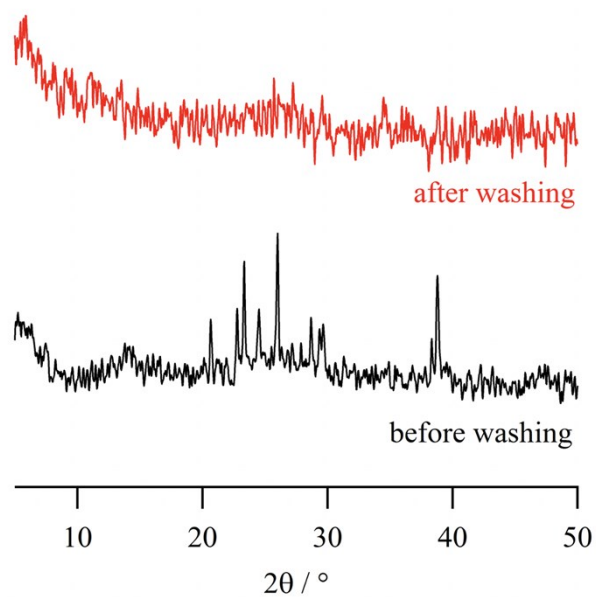


Figure S16. Diffractogram of the polymeric compound measured before and after washing with water.

The p-XRD diffractogram of the crude polymeric compound shows diffraction peaks that are due to CsClO_4 . This crystalline impurity is simply removed by washing the precipitate with water as described in the synthesis. The resulting polymeric material is clearly amorphous.

10. Thermo-Gravimetric Analyses

Representative FT-IR spectra and TGA profile of network samples obtained successively before SQUID measurement (Figure 14a), after SQUID measurement and in-situ drying (Figure 14b), after rehydration (Figure 14c) and after SQUID measurement and in situ-drying (Figure 14d).

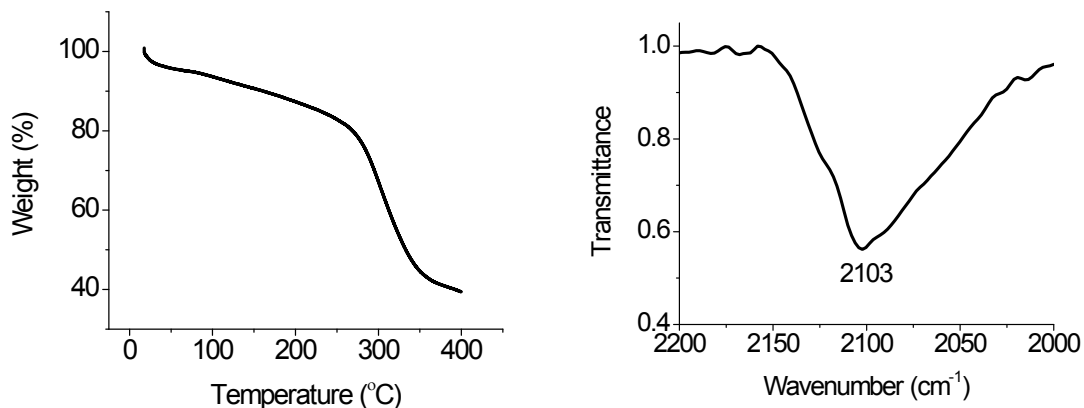


Figure S15a. TGA and IR of the ditopic network before SQUID (Point 1).

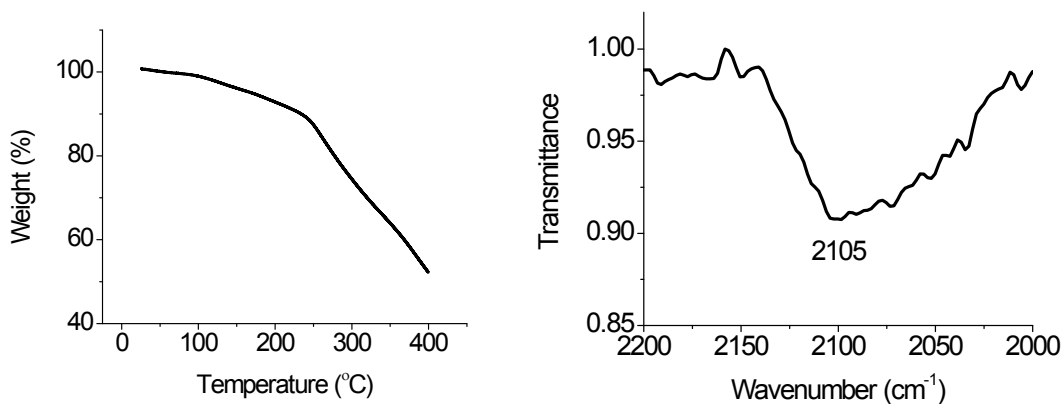


Figure S16b. TGA and IR of the ditopic network after SQUID (Point 2).

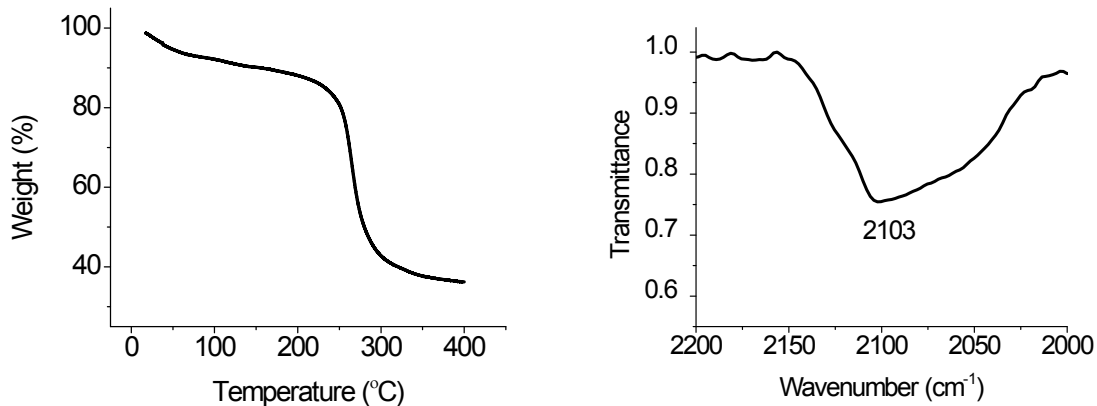


Figure S16c. TGA and IR of the recovered ditopic network (Point 3).

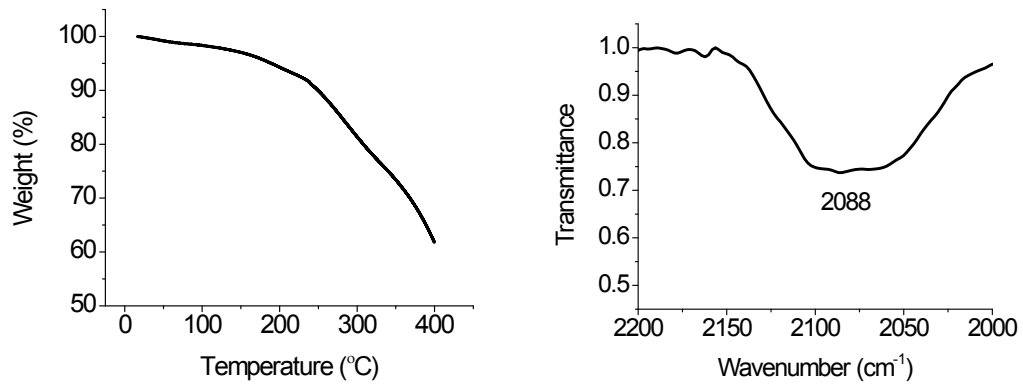


Figure S16d . TGA and IR of the ditopic network after second time in SQUID (Point 4).